RESEARCH ARTICLE

Intracranial myxoid mesenchymal tumors with *EWSR1–CREB* family gene fusions: myxoid variant of angiomatoid fibrous histiocytoma or novel entity?

Tejus A. Bale[1], Angelica Oviedo[2], Harry Kozakewich[3], Caterina Giannini[4], Phani K. Davineni[1], Keith Ligon[1,3], Sanda Alexandrescu [ID][3]

[1] Department of Pathology, Brigham and Women Hospital, Boston, MA.
[2] Department of Pathology Laboratory Medicine, IWK Health Center, Halifax, NS.
[3] Department of Pathology, Boston Children's Hospital, Boston, MA.
[4] Department of Pathology, Mayo Clinic, Rochester, MN.

Abstract

Intracranial myxoid mesenchymal tumor harboring *EWSR1* fusions with *CREB* family of genes was recently described, and it resembles the myxoid variant of angiomatoid fibrous histiocytoma. We present three pediatric patients with intracranial *EWSR1*-rearranged myxoid mesenchymal neoplasm and provide a molecular genetic characterization of these tumors. Clinical histories and imaging results were reviewed. Histology, immunohistochemistry, *EWSR1*, *FUS*, *NR4A3* fluorescence *in situ* hybridization (FISH), and next-generation sequencing (NGS) were performed. A 12-year-old male (case 1), 14-year-old female (case 2), and 18-year-old male (case 3), presented with headaches, emesis, and seizures, respectively. The magnetic resonance images demonstrated tumors abutting the dura (cases 1 and 3) and in the third ventricle (case 2). All tumors were vascular, with solid sheets of monomorphic oval cells in a prominent myxoid/microcystic matrix. A thin fibrous pseudocapsule was present in all lesions, but definitive lymphocytic cuffing was absent. Morphologically, they closely resembled myxoid variant of angiomatoid fibrous histiocytoma. Mitoses were rare, and necrosis was absent. All tumors expressed desmin and GLUT1, and focal EMA and CD99. The proliferation index was low. FISH and NGS showed *EWSR1–CREB1* fusion (cases 1 and 2), and *EWSR1–CREM* fusion (case 3). There were no *FUS* (16p11.2) or *NR4A3* (9q22.33) rearrangements in case 3. Gains of 5q (including *KCNIP1*) and 11q (including *CCND1*) were present in cases 1 and 2. There were no common pathogenic genomic changes other than *EWSR1* rearrangements across cases. CNS myxoid mesenchymal neoplasms with histological and immunophenotypic similarities to myxoid variant of AFH are rare, diagnostically challenging, and harbor *EWSR1–CREB1* and also a novel *EWSR1–CREM* fusion not yet described in AFH. Therefore, it is uncertain if these tumors represent variants of AFH or a new entity. The copy number and mutational changes presented here provide support for future studies to further clarify this issue.

INTRODUCTION

EWSR1 rearrangements with *CREB* family of genes (*CREB1*, *ATF1*, and *CREM*) characterize a spectrum of mesenchymal tumors occurring in a variety of sites and with a wide range of biological behavior. Among them, angiomatoid fibrous histiocytoma (AFH) (3, 8, 10, 11, 23, 25), a tumor of low-to-intermediate malignant potential shows most often *EWSR1–CREB1* fusion as a result of t(2:22)(q33;q12), and less frequently *EWSR1–ATF1* or *FUS–ATF1* resulting respectively from t(12:22)(q13;q12) or t(12;16)(qq13;p11) (8, 9). *EWSR1–CREB1* fusion is the only fusion

described in primary pulmonary myxoid sarcoma to date (14, 20, 27, 28), while *EWSR1–ATF1* fusion has been described in clear cell sarcoma (5, 13); and hyalinizing clear cell carcinoma of salivary gland (4). The myxoid variant of AFH (15, 16, 24) has identical *EWSR1* rearrangements with the classic AFH and is histologically characterized by a rich vascular network and vascular dilatation, epithelioid cells, and a prominent myxoid background. A pseudocapsule and lymphoid aggregates are usually present.

Myxoid AFH had not been reported in the central nervous system, although recently, Kao *et al* (17) described a small series of myxoid mesenchymal tumors that harbor *EWSR1* rearrangements

with *CREB* family of genes, including *CREM* in two cases. The authors hypothesized that these tumors, which show a predilection for intracranial location (4 out of 5 cases), but lack the typical capsular lymphocytic infiltrate and prominent vascular component of AFH myxoid variant, may represent a potentially novel myxoid mesenchymal tumor rather than AFH, myxoid variant. Additional cases with a comprehensive genomic analysis might be needed to support this observation.

This article presents three patients with myxoid mesenchymal intracranial tumors that we encountered in our practice and provides their detailed molecular characterization.

MATERIALS AND METHODS

Clinical history

This study was performed with the approval of the Institutional Review Board at the Boston Children's Hospital and Brigham and Women's Hospital. Case 1 was identified in the archives of Boston Children's Hospital; cases 2 and 3 were encountered in the pathology practice at IWK Health Center, Halifax, NS, and Mayo Clinic, Rochester, MN, respectively. Cases 1 and 2 were presented at the 57th Diagnostic Slide Seminar of the American Association of Neuropathologists in June 2016 (http://neuro.pathology.pitt.edu/ DSSFiles/Current DSS.htm). A summary of the clinical features of all three cases is presented in Table 1.

Case 1: a 12-year-old male presented with mild headache for approximately one month. MRI studies demonstrated a 2.5 cm × 2.3 cm × 1.0 cm, well-defined extra-axial lobulated mass in the left cerebellar hemisphere, abutting the dura (Figure 1a). The past medical history was notable for stage IV adrenal neuroblastoma, diagnosed at age 7 years, for which he was treated with chemotherapy, surgical resection, stem cell transplant and local radiotherapy. There was good response to therapy with no evidence of disease recurrence prior to this presentation. There was no prior cranial radiation. He underwent resection of the cerebellar mass, which was a tan, firm nodule attached to the dura.

Case 2: a 14-year-old female presented with intermittent early morning headache, diplopia, nausea and vomiting. MRI revealed an intra-axial 3.8 cm × 3.6 cm × 3 cm complex solid and cystic contrast-enhancing mass of the posterior left ventricle with surrounding vasogenic edema and slight mass effect (Figure 1b). The resected lesional tissue was firm and tan-pink.

Case 3: an 18-year-old male, presented with a seizure episode. A 3.0 cm × 2.0 cm × 1.5 cm frontal intra-axial circumscribed, lobular mass in the proximity of the superior sagittal sinus, with associated vasogenic edema was found on MRI (Figure 1c). At surgery, the mass was intra-axial well-delineated, firm, tan, and surrounded by a rim of brain parenchyma.

Whole body imaging did not show other lesions in any of the patients.

Histopathology and immunohistochemistry

Hematoxylin–eosin (H&E) stained slides and immunostains were performed according to standard protocols on 4-μm formalin-fixed paraffin-embedded sections using the following primary antibodies and conditions: INI1 (1:100; Ventana Medical Systems, Tuscon, AZ), somatostatin receptor 2A (Epitomics, UMB1, monoclonal, 1:2000); the remainder of the immunohistochemical stains were performed using automated staining with commercially available prediluted antibodies (EMA, S100, desmin, Glut-1, GFAP, Olig2, SOX10, synaptophysin, myogenin, smooth muscle actin [SMA], CD68, keratin, CD34, CD99; Leica Biosystems, Buffalo Grove, IL). Counterstaining for nuclei was performed using Mayer's hematoxylin and coverslips were mounted with Permount (Fisher Scientific). Photographs were taken using an Olympus BX41 microscope and an Olympus DP25 camera.

Fluorescence *in situ* hybridization (FISH) analysis

FISH was performed on 4-μm paraffin sections according to standard protocols (29). *EWSR1* (22q12) rearrangement was evaluated using the Vysis LSI *EWSR1* break-apart Probe kit (Abbott Molecular, Des Plaines, IL). Also, FISH for *FUS* (16p11.2) and *NR4A3* (9q22.33) were pursued for case 3 using commercially available dual-color break-apart probes (BAP).

Next-generation sequencing

DNA was isolated from tissue containing at least 20% tumor nuclei and analyzed by massively parallel sequencing using a solution-phase Agilent SureSelect hybrid capture kit using methods previously described (19). Somatic mutations in tumor DNA were detected using the exome-sequencing platform OncoPanel (Illumina HiSeq) in a CLIA-certified laboratory. The OncoPanel assay detects mutations in 300 different cancer genes and 113 introns

Table 1. Clinical and radiological characteristics of the three patients.

| Case	Age	Sex	Symptoms	MRI—location of lesion	MRI—tumor size (greatest dimension)	Other MRI findings
1	12	M	Headache	Posterior fossa/cerebellar, abutting dura	2.5 cm × 2.3 × cm 1.0 cm	Lobulated, heterogeneous appearance, contrast enhancing, no tail-sign present
2	14	F	Headache, nausea, vomiting, diplopia	Intraventricular (left lateral)	3.8 cm × 3.6 cm × 3 cm	Heterogeneous appearance, surrounding vasogenic edema and mass effect
3	18	M	Generalized tonic-clonic seizures	Midline/right frontal (falx area), surrounded by a thin rim of brain parenchyma	3.0 cm × 2.0 cm × 1.5 cm	Contrast enhancing, surrounding vasogenic edema, no definitive dural attachment
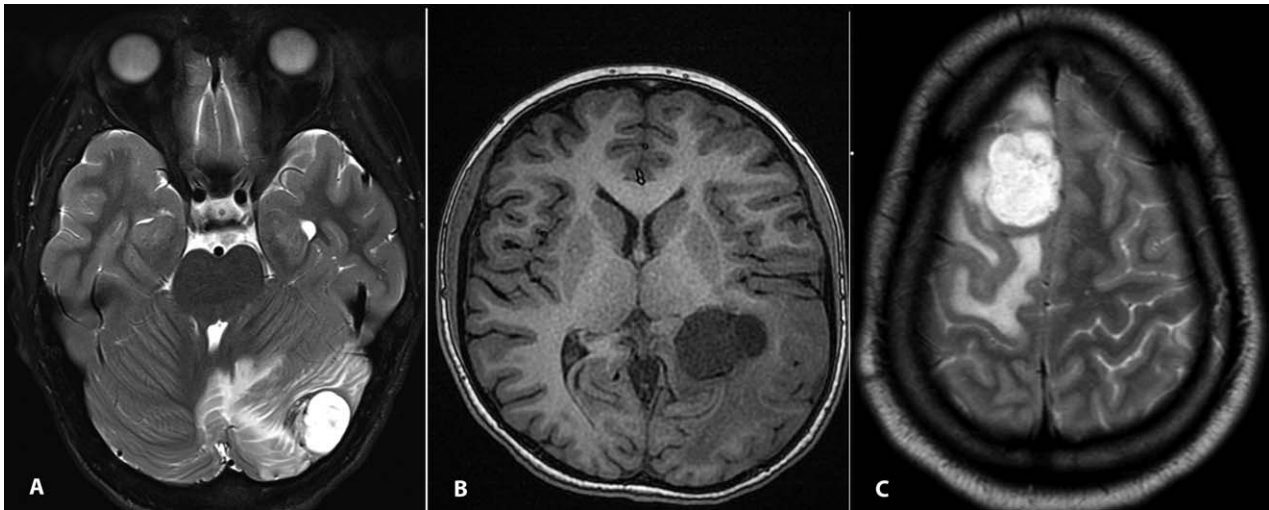
Figure 1. a. Case 1—axial T2-hyperintense well-demarcated tumor in right cerebellar hemisphere with surrounding edema, abutting the dura. **b.** Axial T1 MRI of case 2 shows well-demarcated tumor involving left posterior horn of lateral ventricle. **c.** Case 3—axial T2-hyperintense tumor in left frontal region, having similar features to those in case 1, but no definitive attachment to dura.

across 35 genes for rearrangement detection. Common single nucleotide polymorphisms (SNP) were accounted for using the following informatic steps: any SNP present at >0.1% in Exome Variant Server (NHLBI GO Exome Sequencing Project [ESP], Seattle, WA; URL: http://evs.gs.washington.edu/EVS/) or present in dbSNP was filtered. Variants also present in the COSMIC mutation database were rescued for manual review. Individual variants present at <10% allele fraction or in regions with <50× coverage were flagged for manual review. In an attempt to identify potential damaging effects of missense mutations, computational predictions of the impact of protein sequence variants were made using the software tool PolyPhen-2 (2). Structural variants were detected using the BreaKmer algorithm, which identifies rearrangements and nucleotide-level breakpoints by realigning variant contigs generated from assembling all misaligned reads within the targeted NGS data (1).

RESULTS

Light microscopic features

The H&E-stained sections of all tumors demonstrated a myxoid neoplasm of moderate cellularity (Figure 2a) with focal vague nodular architecture and hypocellular areas rich in collagen (Figure 2b). The cells were monomorphic and mildly atypical, growing in irregular trabecular (Figure 2c). A thin fibrous capsule was seen in all tumors (Figure 2d). The cells had oval-to-spindled nuclei, speckled chromatin, and moderate amounts of eosinophilic cytoplasm and were occasionally arranged in whorls (Figure 2e). Although the tumors had foci demonstrating a rich capillary network (Figure 2f), rare thin-walled dilated vessels resembling lakes of blood were seen only in case 3 (Figure 2b). A discrete angiocentric pattern of growth was present particularly in case 1 (Figure 2g). Invasion of the brain and necrosis were not present, and mitoses were rare in cases 2 and 3. Case 1 had a single focus with up to 6 mitoses/10 high power fields. Well-developed lymphocytic cuffing was not present in any of the cases. Occasional collagenous fibers similar to amianthoid fibers were present in every tumor, but without rosetting or sunburst appearance (Figure 2h).

Immunohistochemistry

All three tumors demonstrated extensive (more than 90% tumor cells) and strong immunopositivity for desmin (Figure 3a) and GLUT-1 (Figure 3b). The EMA (Figure 3c) and CD99 (Figure 3d) immunostains were focally positive in a cytoplasmic and membranous pattern, respectively. The S100, SOX10, CD34, SSTR2A, myogenin, GFAP, OLIG2, synaptophysin, and CAM5.2 immunostains were negative. Pale, variable and focal SMA expression was present in all three tumors in a cytoplasmic and membranous pattern that was considered nonspecific (not illustrated). Focal CD68 expression was present only in case 2. A CD68 immunostain was not performed in case 3. The proliferation labeling index, as demonstrated by the Ki67 immunostain, was low (less than 5%) with the exception of the focus in case 1, where the rate was up to 12%; however, due to the number of macrophages and occasional inflammatory cells, this value might be an overestimate. INI1 (BAF47) nuclear immunopositivity was retained in all three tumors.

Molecular genetic analysis

FISH demonstrated *EWSR1* (22q12) rearrangement in 88% of nuclei in case 1, 93% of nuclei in case 2, and 63% of nuclei in case 3. FISH for *FUS* (16p11,2) and *NR4A3* (9q22.33) was negative for rearrangements in case 3.

Targeted exome sequencing with subsequent structural variation analysis using the BreaKmer algorithm detected a reciprocal chromosomal rearrangement between chromosome 2 (mapping to intron 6 in case 1 and intron 7 in case 2) of *CREB1* and chromosome 22 (mapping to intron 8 in cases 1 and 2) of *EWSRI* in cases 1 and 2. In case 3, BreaKmer identified a fusion between *EWSR1* (mapping to intron 9) and *CREM* (mapping to intron 3) on chromosome 10 (Figure 4).
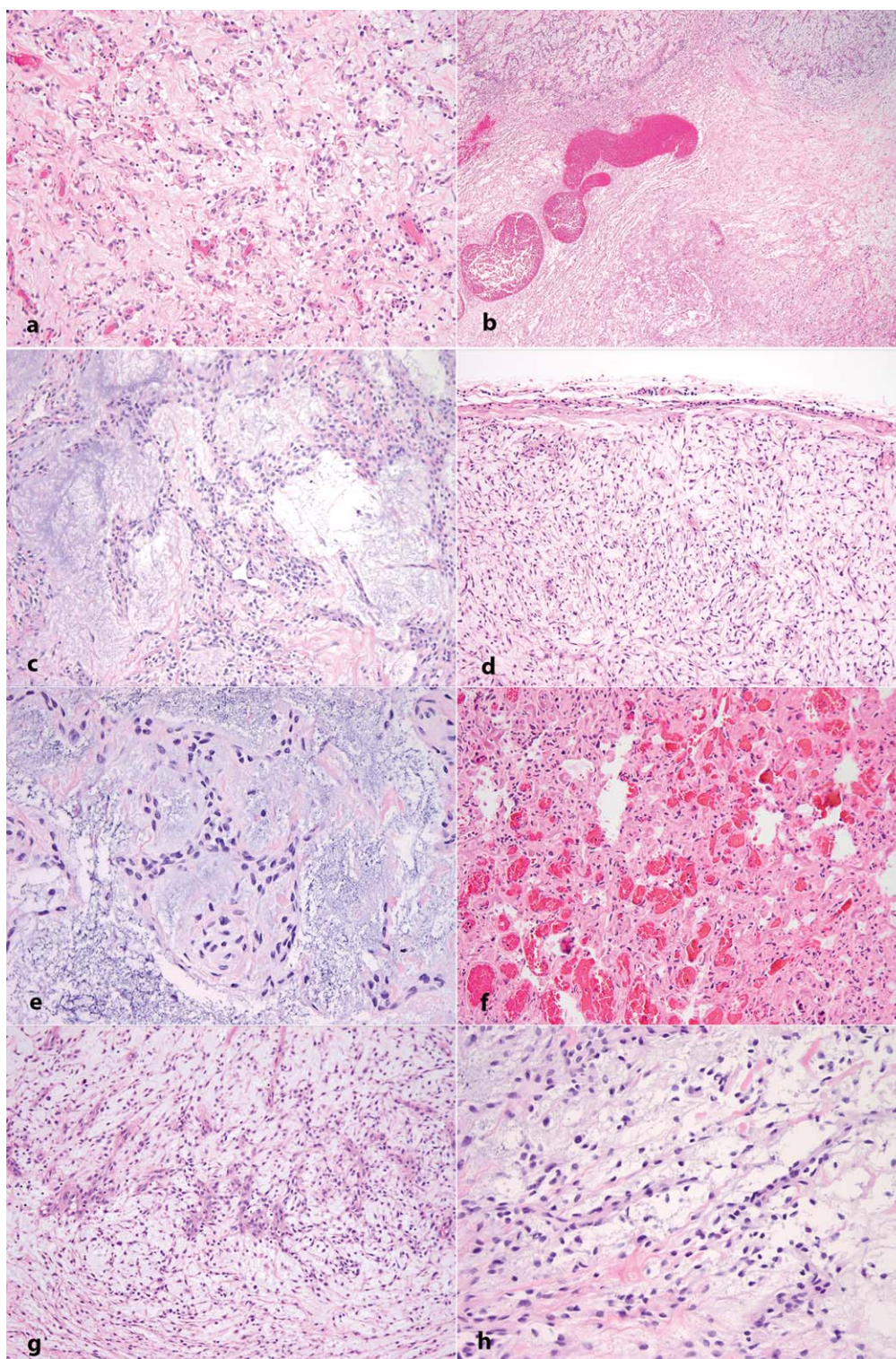
Figure 2. *Histological characteristics.* **a.** Hematoxylin–eosin-stained section representative of the three tumors, showing epithelioid neoplasm composed of round-to-oval cells growing in short cords in a prominent myxoid background. **b.** A vague nodular pattern admixed with hypocellular areas rich in collagen, and occasional prominent vessels. **c.** Short cords and trabecula of monomorphic cells in a prominent myxoid background with scattered collagen fibers. **d.** The tumors were surrounded by a thin fibrous capsule. **e.** Cords and occasional whorls composed of monomorphic oval-to-spindle cells with minimal atypia in a prominent myxoid background. **f.** Focus of rich capillary network (more prominent in case 2). **g.** Discrete angiocentric pattern (more prominent in case 1). **h.** Spindle and stellate cells with collagen fibers resembling amianthoid fibers.
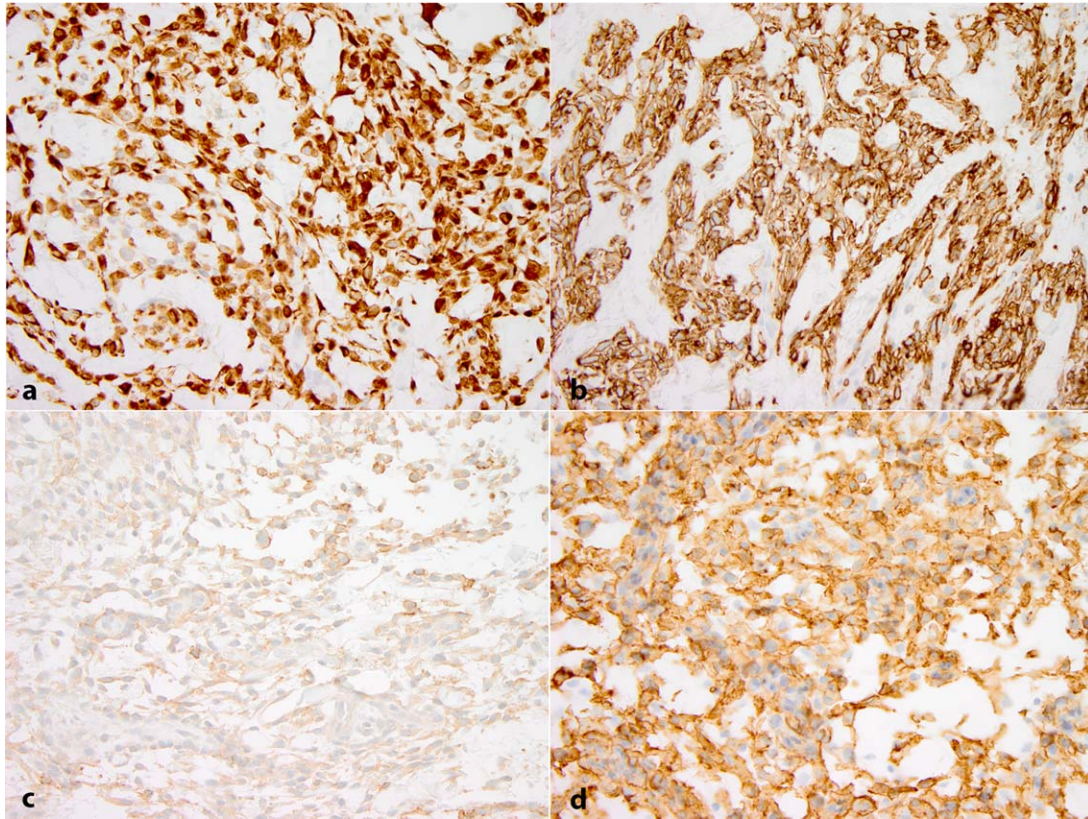
Figure 3. *Immunohistochemical profile*. Desmin (**a**) and Glut-1 (**b**) immunostains diffusely and strongly positive, EMA (**c**) expressed in subset of tumor cells, CD99 immunostain (**d**) positive in a membranous pattern in large number of lesional cells.

Copy number alterations detected by NGS demonstrated low-level gains of 5q (including *KCNIP1*, 5q35.1) and 11q (including *CCND1*) in cases 1 and 2. The 5q gains in case 1 also involved 5q32 (including *CSF1R* and *PDGFRB*). Case 1 also demonstrated single copy deletions of 12p (including *CCND2)* and 19p (*ZNF708*). Additional alterations in case 2 included low copy number gains involving 15q (including *NTRK3*) and 18q (including *GATA6*). With the exception of the rearrangement in *EWSR1*, no additional copy number alterations were identified in case 3.

No single nucleotide variants previously reported in the COSMIC cancer database (http://cancer.sanger.ac.uk/cosmic) were found in these three cases (Table 2). Several novel variants were however noted, but the majority of these occurred at allelic fractions consistent with normal germline variants. There were no common single nucleotide variants identified in the three cases. Of interest is the *BRAF c.2128-5dupT* mutation observed in 8% of 325 reads in case 2, as *BRAF* mutations have not been described in *EWSR1*-rearranged tumors, and such finding might have therapeutic implications.

To explore if these copy number changes and nucleotide variants might overlap with those seen in classic AFH, which has not been sequenced at this level, we identified in the archives at Boston Children's Hospital four cases of AFH in the 2012–2014 interval, of which one had available NGS. The patient was an 8-year-old boy with a classic AFH of the scalp. Aside from an *EWSR1–ATF1* fusion demonstrated by BreaKmer analysis, there were no significant copy number changes. The nucleotide variants identified in

this case are included in Table 3. None of the mutations found in this classic AFH were known to be pathogenic and none were reported previously in COSMIC. There was no significant overlap with the genomic findings of the three myxoid mesenchymal tumors.

At 1-year follow-up, all three patients were well, without evidence of recurrence.

DISCUSSION

We describe three unusual myxoid mesenchymal tumors occurring intracranially in young patients, characterized by a peculiar myxoid morphology and showing *EWSR1* rearrangements, closely resembling the cases recently described by Kao *et al* (17). Because of the histological features and chromosomal rearrangements seen in our three cases, the initial interpretation was of myxoid variant of AFH. Myxoid variant of AFH (15, 16, 24, 25) carries low-to-intermediate malignant potential, with reportedly only rare patients developing local recurrence; no distant metastases are reported. As in the classic AFH, the majority of the *EWSR1* rearrangements in the myxoid variant involve fusion of *EWSR1–CREB1*. Less commonly, the *EWSR1* rearrangement results from t(12;22)(q13;q12) leading to *EWSR1–ATF1* (7, 16). Rare examples of intracranial classic AFH, extra-axial and intra-axial parieto-occipital, have been reported in the literature (6, 9, 12, 22), albeit none of these cases had myxoid features on histology. In the series of myxoid variant of AFHs
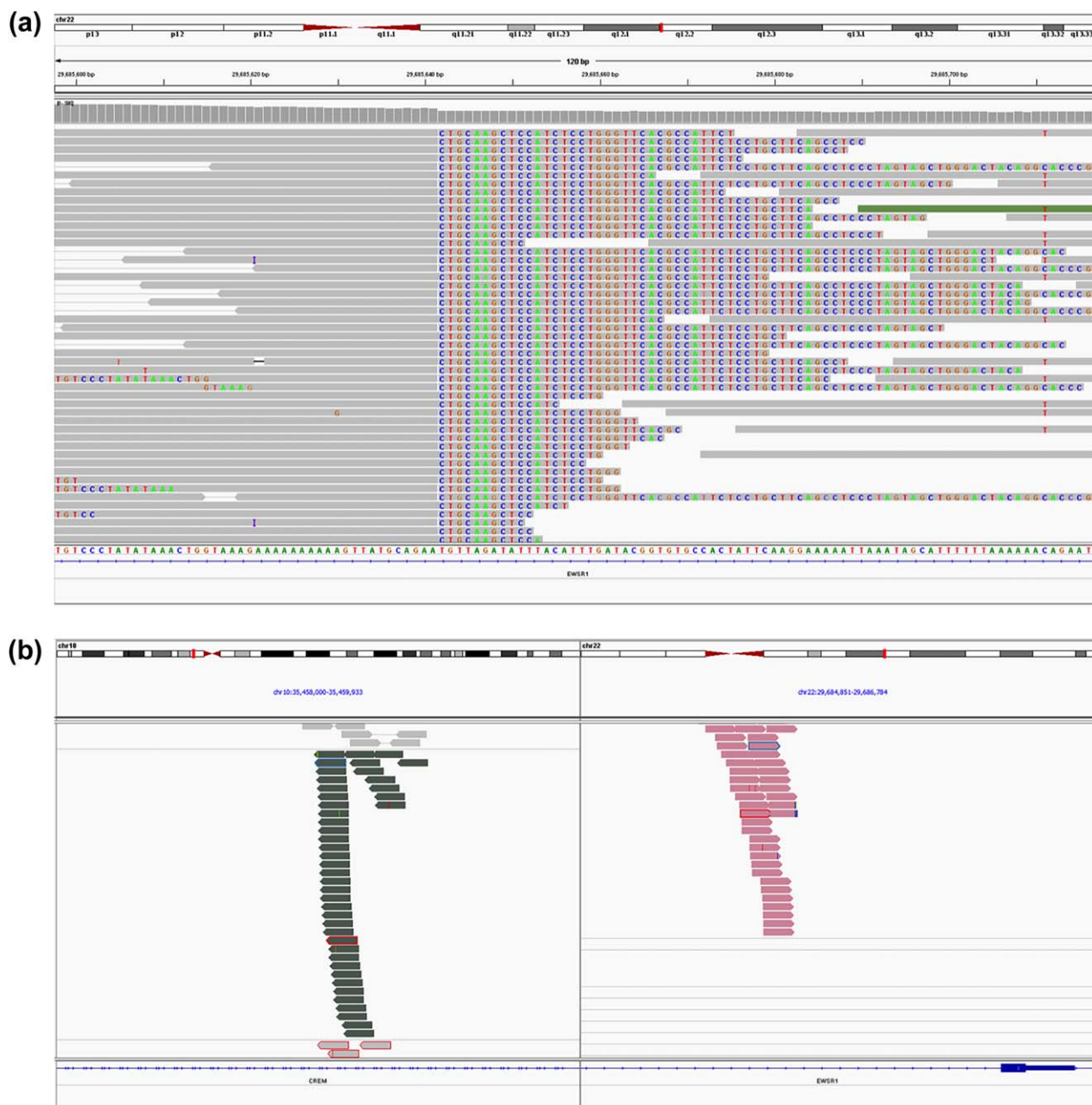
Figure 4. The EWSR1–CREM fusion in case 3 is supported by discordant read pairs indicating a break in EWSR1 (**a**) and alignment of split reads to EWSR1 and CREM (**b**) as predicted by the translocation analysis tool BreaKmer.

described in the literature, none occurred intracranially. Of note, 1 of the 21 cases in the series of Schaefer et al. lacked a fibrous capsule and lymphocytic pseudocapsular cuffing, and blood-filled cystic spaces were not present in 4 of the 21 cases. In a more recent series of 21 cases of AFH, Shi *et al* (25) found eight tumors that lacked pseudoangiomatoid spaces; two of these had prominent myxoid stroma, and one of these had prominent scleroting stroma. These series provide supportive evidence for a relatively wide histologic spectrum of AFH, which might challenge the hypothesis that these tumors represent a new entity.

The differential diagnosis of such myxoid mesenchymal tumors is wide; in our series, other entities with similar histology and *EWSR1* rearrangements were largely excluded by immunohistochemical studies: myoepithelial tumors—negative cytokeratin, GFAP, equivocal SMA; microcystic meningioma with myxoid changes—negative somatostatin receptor 2A; an unusual glial or glioneuronal neoplasm—negative OLIG2, synaptophysin; extraskeletal myxoid chondrosarcoma—negative S100, and also by additional FISH studies in case 3 (no *NR4A3* rearrangements for extraskeletal myxoid chondrosarcoma and *FUS* rearrangements for

Table 2. Variants detected by targeted NGS (OncoPanel).

	Gene	DNA variant	Amino acid change	Variant type	Allelic fraction	Functional effect	PolyPhen-2 functional effect prediction score
Case 1	**PRF1**	**c.529C>T**	**p.R177C**	**Missense**	**0.40**	**Probably damaging**	0.999
	MLH1	c.409G>C	p.A137P	Missense	0.43	Benign	0.169
	MECOM	**C.332G>C**	**p.G111A**	**Missense**	**0.45**	**Probably damaging**	**1**
	FANCD2	c.2309A>G	p.K770R	Missense	0.46	Benign	0.171
	ROS1	**c.6074T>A**	**p.I2025N**	**Missense**	**0.46**	**Probably damaging**	1
	ATM	**c.1726A>G**	**p.I576V**	**Missense**	**0.48**	**Possibly damaging**	**0.675**
	CDKN2C	c.80A>G	p.N27S	Missense	0.48	Benign	0.001
	SDHA	c.728C>T	p.S243F	Missense	0.49	Benign	0.146
Case 2	**BRAF**	**c.2128–5dupT**	–	**Frameshift**	**0.08**	**Disrupts protein tyrosine kinase domain at p.457-714**	–
	GLI2	c.178G>C	p.A60P	Missense	0.43	Benign	0.003
	KMT2D	**c.787C>T**	**p.R263C**	**Missense**	**0.53**	**Probably damaging**	**0.99**
Case 3	NF1	c.3160A>C	p.N1054H	Missense	0.03	Benign	0.017
	TCF3	c.1080C>A	p.P360P	Silent	0.37	–	–
	BRCA1	c.2779G>T	p.A927S	Missense	0.49	Benign	0.367
	ERCC5	c.1810G>T	p.V604L	Missense	0.49	Benign	0.001
	ERBB3	c.3334delG	p.V1112Cfs*29	Frameshift	0.50	Disrupts sequence distal to the protein tyrosine kinase domain	–
	CUX1	**c.1653G>A**	**p.M551I**	**Missense**	**0.51**	**Probably damaging**	**0.966**
	STAT6	c.1213–8C>G	–	Frameshift	0.54	–	–
	PRAME	c.21 + 889G>A	–	Frameshift	0.64	–	–

Missense mutational effects are assessed by PolyPhen-2 prediction of functional effects of human nsSNPs (2). Frameshift mutational effects are determined by gene analysis using COSMIC and Pfam (proteins family database). Potentially deleterious variants are indicated in bold.

low grade fibromyxoid sarcoma) before NGS was performed. Myxoid AFH and primary pulmonary myxoid sarcoma (PPMS) have similar morphology, immunoprofile, and chromosomal rearrangements, and Smith *et al* documented these features in a brief three case series (26). Desmin immunostain is usually used as a method to distinguish between myxoid AFH (diffuse positivity) and PPMS (usually negative) (29). However, Smith *et al* describes one case of *EWSR1*-rearranged potential PPMS with desmin expression. Although in this particular case, the *EWSR1* fusion partner was not *ATF1* or *CREB1*, the immunoprofile overlap raises the possibility that these two entities might be part of a single diagnostic spectrum; a more comprehensive molecular characterization of cases of PPMS and AFH might provide further evidence in that direction.

A curious finding was that all three tumors demonstrated extensive strong positivity for GLUT1 (Figure 3b), which has not been

reported in AFH or in the recent series of five cases of myxoid mesenchymal tumor with *EWSR1* rearrangements and predilection for CNS.

The tumors in our study are similar to those described by Kao *et al*. Notably, the similarities include occurrence in adolescents, intra- and extra-axial locations (posterior fossa, intraventricular, frontal-midline areas), and histological and immunohistochemical profile. In contrast, however, the tumors in our series demonstrated focal histologic features of classic AFH, within the prominent myxoid background: rich vascular meshwork and occasional dilated vascular spaces, thin fibrous pseudocapsule, and minimal lobular architecture. In addition, the immunoprofile of the cases in our series is identical to that of AFH (EMA and desmin expression and focal membranous CD99 positivity), and therefore, we are not entirely sure that they represent a new entity that is biologically distinct of the myxoid variant of AFH.

Two of our cases demonstrated the more common *EWSR1–CREB1* fusion of AFH. The *EWSR1–CREM* fusion observed in case 3 has not been described in AFH, but was present in one intracranial case described by Kao *et al*. *CREB1* and *CREM*, along with *ATF1*, are part of a related family of transcription factors with similar structure and function, but the significance of *CREM* as a fusion partner is unclear (18, 21); it is not unique to CNS located tumors as it was present in the index perirectal myxoid mesenchymal neoplasm.

In addition to the characterization of the fusions in our tumors, we also encountered low-level copy number gains involving chromosomes 5q (including *KCNIP1*, 5q35.1) and 11q (including

Table 3. Mutations identified by targeted NGS (OncoPanel) in one case of a classic AFH in the scalp of an 8-year-old male.

Gene	DNA variant	Amino acid change	Variant type	Allelic fraction
ESR1	c.227C>G	p.T76S	Missense	0.48
FANCA	c.893 + 101G>A	–	Intronic	0.49
KMT2D	c.6235–6C>G	–	Intronic	0.5
PRPF8	c.*72C>G	–	Intronic	0.48
ROS1	c.1757C>G	p.A586G	Missense	0.42
STAT3	c.714G>C	p.E238D	Missense	0.41

CCND1) in both cases 1 and 2. Also, in case 1, the 5q gains involved 5q32 (including *CSF1R* and *PDGFRB*), and a single copy deletion of 12p (including *CCND2*) and 19p (*ZNF708*) were also present. Additional alterations in case 2 included low copy number gains of 15q (including *NTRK3*) and 18q (including *GATA6*). There were no copy number changes present in case 3. Copy number alterations have not been previously reported in AFH and were not present in the classic AFH with available NGS results included in this study.

A single mutational signature was not identified in these three cases (Table 2). Moreover, no variants of definitive significance in cancer were detected. As the tissue was analyzed in the absence of paired non-tumor controls from the same patient, the possibility that these variants represent normal germline variants cannot be entirely excluded. However, the frameshift mutation in *BRAF* present in case 2, although not reported in cancer, is of interest, given the importance of *BRAF* alterations in the pathogenesis of many tumors, including pediatric brain tumors. An extensive molecular characterization of classic and myxoid variant AFH and of myxoid mesenchymal tumor described recently has not been published to date. In the classic AFH of the scalp reviewed by us, although there were no nucleotide variants reported in cancer, a *ROS1* missense mutation (c.1757C>G, pA586G) was present. A *ROS1* (c.6074T>A, pI576V) missense mutation was also present in case 1, and was absent in the other two tumors. Also a *KMT2D* intronic variant (c.6235-6C>G) was seen in the classic AFH, and a missense *KMT2D* mutation (c.789C>T, p.R263C) was seen in case 2. Although these mutations are not identical, and their effect in cancer is not described, their occurrence in both classic AFH and in an intracranial myxoid mesenchymal tumor with similar biology to myxoid variant of AFH, is worthy of consideration in future studies, as they might suggest biological overlap.

In conclusion, we report three cases of intracranial myxoid mesenchymal tumors with *EWSR1* fusions with *CREB1* and *CREM*, and provide further insight in the genomics of these tumors. While signature copy number changes and single nucleotide variants were not identified, this extensive molecular characterization was not reported in these tumors or in AFH. The presence of a *BRAF* mutation in one of the cases might be of therapeutic interest. This is the second series of such tumors, the first one containing only four (out of five) intracranial cases; therefore, our study provides further promising support for this entity with a challenging differential diagnosis for the neuropathologists.

ACKNOWLEDGMENTS

REFERENCES

1. Abo RP, Ducar M, Garcia EP, Thorner AR, Rojas-Rudilla V, Lin L *et al* (2015) BreaKmer: detection of structural variation in targeted massively parallel sequencing data using kmers. *Nucleic Acids Res* **43**: e19. doi:10.1093/nar/gku1211.

2. Adzhubei I, Jordan DM, Sunyaev SR (2013) Predicting functional effect of human missense mutations using PolyPhen-2. *Curr Protoc Hum Genet* **Chapter 7**;Unit 7.20.

3. Antonescu CR, Dal CP, Nafa K, Teot LA, Surti U, Fletcher CD, Ladanyi M (2007) EWSR1–CREB1 is the predominant gene fusion in angiomatoid fibrous histiocytoma. *Genes Chromosomes Cancer* **46**: 1051–1060.

4. Antonescu CR, Katabi N, Zhang L, Sung YS, Seethala RR, < Jordan RC, Perez-Ordonez B *et al*, (2011) EWSR1ATF1 fusion is a novel and consistent finding in hyalinizing clear-cell carcinoma of salivary gland. *Genes Chromosomes Cancer* **50**:559–570.

5. Antonescu CR, Nafa K, Segal NH, Dal Cin P, Ladanyl MEWS-CREB1 (2006) a recurrent variant fusion in clear cell sarcoma—association with gastrointenstinal location and absence of melanocytic differentiation. *Clin Cancer Res* **12**:5356–5362.

6. Ashareef MA, Almadidy Z, Baker T, Perry A, Welsh CT, Vandergrift WA 3rd. (2016) Intracranial angiomatoid fibrous histiocytoma: case report and literature review. *World Neurosurg* **96**:403–409.

7. Chen G, Folpe AL, Colby TV, Sittampalam K, Patey M, Chen MG, Chan JK (2011) Angiomatoid fibrous histiocytoma: unusual sites and unusual morphology. *Mod Pathol* **24**:1560–1570.

8. Costa MJ, Weiss SW (1990) Angiomatoid malignant fibrous histiocytoma. A follow-up study of 108 cases with evaluation of possible histologic predictors of outcome. *Am J Surg Pathol* **14**: 1126–1132.

9. Dunham C, Hussong J, Seiff M, Pfeifer J, Perry A (2008) Primary intracerebral angiomatoid fibrous histiocytoma: report of a case with a t(12;22)(q13;q12) causing type 1 fusion of the EWS and ATF-1 genes. *Am J Surg Pathol* **32**:478–484.

10. Enzinger FM (1979) Angiomatoid malignant fibrous histiocytoma: a distinct fibrohistiocytic tumor of children and young adults simulating a vascular neoplasm. *Cancer* **44**:2147–2157.

11. Fanburg-Smith JC, Miettinen M (1999) Angiomatoid "malignant" fibrous histiocytoma: a clinicopathologic study of 158 cases and further exploration of the myoid phenotype. *Hum Pathol* **30**:1336–1343.

12. Hansen JM, Larsen VA, Scheie D, Perry A, Skjoth-Rasmussen J (2015) Primary intracranial angiomatoid fibrous histiocytoma presenting with anaemia and migraine-like headaches and aura as early clinical features. *Cephalalgia* **35**:1334–1336.

13. Hisaoka M, Ishida T, Kuo TT, Matsuyama A, Imamura T, Nishida K *et al* (2008) Clear cell sarcoma of soft tissue: a clinicopathologic, immunohistochemical, and molecular analysis of 33 cases. *Am J Surg Pathol* **32**:452–460.

14. Jeon YK, Moon KC, Park SH, Chung DH (2014) Primary pulmonary myxoid sarcomas with EWSR1CREB1 translocation might originate from primitive peribronchial mesenchymal cells undergoing myofibroblastic differentiation. *Virchows Arch* **465**:456–461.

15. Justin Wong SB, Wee A, Puhaindran ME, Pang B, Lee VK (2015) Angiomatoid fibroys histiocytoma with prominent myxoid stroma: a case report and review of the literature. *Am J Dermatopathol* **37**: 623–631.

16. Kao YC, Lan J, Tai HC, Li CF, Liu KW, Tsai JW *et al* (2014) Angiomatoid fibrous histiocytoma: clinicopathological and molecular characterization with emphasis on variant histomorphology. *J Clin Pathol* **67**:210–215.

17. Kao YC, Sung YS, Zhang L, Chen CL, Vaiyapuri S, Rosenblum MK, Antonescu CR (2016) EWSR1 fusions with CREB family transcription factors define a novel myxoid mesenchymal tumor with predilection for intracranial location. *Am J Surg Pathol* **41**:482–490.

18. Lonze BE, Ginty DD (2002) Function and regulation of CREB family transcription factors in the nervous system. *Neurib* **35**:605–623.

19. MacConaill LE, Campbell CD, Kehoe SM, Bass AJ, Hatton C, Niu L *et al* (2009) Profiling critical cancer gene mutations in clinical tumor samples. *PLoS ONE* **4**:e7887.

20. Matsukuma S, Hisaoka M, Obar K, Kono T, Takeo H, Sato K, Hata Y (2012) Primary pulmonary myxoid sarcoma with EWSR1CREB1 fusion, resembling extraskeletal myxoid chondrosarcoma: case report with a review of literature. *Pathol Int* **62**:817–822.

21. Mayr B, Montmini M (2001) Transcritional regulation by the phosphorylation-dependent factor CREB. *Nat Rev Mol Cell Biol* **2**:599–609.

22. Ochalski PG, Edinger JT, Horowitz MB, Stetler WR, Murdock GH, Kassam AB, Engh JA (2010) Intracranial angiomatoid fibrous histiocytoma presenting as recurrent multifocal intraparenchymal hemorrhage. *J Neurosurg* **112**:978–982.

23. Rossi S, Szuhai K, Ijszenga M, Tanke HJ, Zanatta L, Sciot R *et al* (2007) EWSR1CREB1 and EWSR1ATF1 fusion genes in angiomatoid fibrous histiocytoma. *Clin Cancer Res* **13**:7322–7328.

24. Schaefer IM, Fletcher CD (2014) Myxoid variant of so-called angiomatoid "malignant fibrous histiocytoma": clinicopathologic characterization. A series of 21 cases. *Am J Surg Pathol* **38**:816–823.

25. Shi H, Li H, Zhen T, Zhang F, Dong Y, Zhang W, Han A (2015) Clinicopathological features of angiomatoid fibrous histiocytoma: a series of 21 cases with variant morphology. *Int J Clin Exp Pathol* **8**:772–778.

26. Smith SC, Palanisamy N, Betz BL, Tomilins SA, Mehra R, Schmidt LA *et al* (2014) At the intersection of primary pulmonary myxoid sarcoma and pulmonary angiomatoid fibrous histiocytoma: observations from three new cases. *Histopathology* **65**:144–146.

27. Thway K, Fisher C (2012) Tumors with EWSR1CREB1 and EWSR1ATF1 fusions: the current status. *Am J Surg Pathol* **36**:e1–e11.

28. Thway K, Nicholson AG, Lawson K, Gonzalez D, Rice A, Balzer B *et al* (2011) Primary pulmonary myxoid sarcoma with EWSR1-CREB1 fusion: a new tumor entity. *Am J Surg Pathol* **35**:1722–1732.

29. Weremowicz S, Schofield DE (2007) Preparation of cells from formalin-fixed, paraffin-embedded tissue for use in fluorescence in situ hybridization (FISH) experiments. *Curr Protoc Hum Genet* **Chapter 8**:Unit 8.8.